applied sciences

MDPI

Article

Fragility Curves for Material Characteristics and Damage Index for Brick Masonry Exposed to Freeze–Thaw Action

Mojmir Uranjek, Matjaž Skrinar, Denis Imamović and Iztok Peruš *

Faculty of Civil Engineering, Transportation Engineering and Architecture, University of Maribor, Smetanova 17, 2000 Maribor, Slovenia; mojmir.uranjek@um.si (M.U.); matjaz.skrinar@um.si (M.S.); denis.imamovic@um.si (D.I.)
* Correspondence: iztok.perus@um.si; Tel.: +386-(2)-22-94-361

Abstract: In regions exposed to floods followed by cold weather, brick masonry as a structural basis of the building envelope can be damaged due to the accompanying phenomenon of freezing and thawing. The main purpose of the article is the development of a mathematical model able to predict the chosen mechanical parameters and damage index of brick wallets for a given number of freeze-thaw cycles. For this, a statistical model derived from experimental data is used. As a result, regression curves for Young's modulus and ductility for two types of mortar are obtained. Furthermore, fragility curves for ductility and also the damage index, which is based on displacement ductility, are presented. The obtained results enable probabilistic risk assessments in the case of deteriorated ductility and increased damage on brick masonry due to freeze–thaw cycles.

Keywords: freezing/thawing; brick wallets; experimental; statistical model; fragility curve; damage index

check for updates

Citation: Uranjek, M.; Skrinar, M.; Imamović, D.; Peruš, I. Fragility Curves for Material Characteristics and Damage Index for Brick Masonry Exposed to Freeze–Thaw Action. *Appl. Sci.* **2021**, *11*, 10027. https://doi.org/10.3390/app112110027

Academic Editor: Stojan Kravanja

Received: 2 August 2021
Accepted: 21 October 2021
Published: 26 October 2021

Publisher's Note: MDPI stays neutral with regard to jurisdictional claims in published maps and institutional affiliations.

Copyright: © 2021 by the authors. Licensee MDPI, Basel, Switzerland. This article is an open access article distributed under the terms and conditions of the Creative Commons Attribution (CC BY) license (https://creativecommons.org/licenses/by/4.0/).

1. Introduction

The phenomenon of freezing and thawing, especially in regions exposed to floods, can significantly influence the properties of the building envelope. Walls, especially brick masonry ones, which can be saturated with water due to flooding in the rainy autumn period and exposed to cycles of freezing and thawing (labeled F/T in the rest of the text) due to the cold winter that follows the rainy season, may experience damage and a consequent reduction in mechanical properties. Freezing occurs in porous and permeable materials in the presence of water at temperatures below 0 °C. Frost resistance represents the ability of moistened material to resist F/T cycles without damage. It depends on the climatic conditions, thermal conductivity, water absorption, and porosity [1]. The phenomenon and the mechanisms of deterioration of materials due to F/T are dealt with by three main theories: the hydraulic pressure theory, closed container theory, and ice lence growth theory, which are described in [2–4]. Many contributions in the literature deal with the influence of F/T on mortar, brick, and plaster as the constituent components of the wall [5–8]. Considerably less authors have studied the influence of F/T on the mechanical properties of the wall as the composite [9] as well as the mathematical models that describe the dependence of mechanical properties and level of damage depending on F/T action [10]. We are often faced with complex and expensive experiments, in which it is hard to modify and adjust all variables that occur in the observed phenomena. Therefore, mechanical properties are generally not determined from experimental measurements, but by using suitable physical models, which are then experimentally verified. In the case of complex phenomena, such as cyclic F/T of brick masonry, ordinary physical models are unreliable and inaccurate due to uncertainty in the material, execution, and complex dynamic processes that take place in the experiment and nature. We attempt to achieve satisfactory description with optimally designed experiments where key variables are changed, and then the phenomenon is described by statistical tools using engineering logic and the integration of knowledge of individual physical models. The latest approach, which was also used in this paper, corresponds to a so-called problem of »small data«,

which is about finding the causation, the reason why, in contrast to the problem of »big data«, which is about finding correlations in enormous amounts of data [11] (which are typically not available in structural engineering). The purpose of this paper is to develop a mathematical model based on the experimental results, which will be able to predict key mechanical characteristics and the damage index for a given number of F/T cycles by different qualities/types of mortar, taking into account uncertainties in the data and results. The article presents results obtained on brick wallets built with pure lime mortar as well as wallets built with lime mortar with the addition of ground granulated blastfurnace slag.

2. Materials and Methods

2.1. Experimental Part

The influence of F/T action on the wall as a composite was studied by experiments presented in [9]. Here, only basic information on the experiment is provided, and detailed description is given elsewhere [9]. Two different types of mortar were used for the construction of wallets exposed to 50 and 150 F/T cycles: mortar M1 made from lime putty and mortar M3a, where 40% (by mass) of ground granulated blastfurnace slag was added according to the share of dry binder in lime putty. In both cases, a volumetric ratio lime putty:sand of 1:3 was taken into account. Although the hardening processes of the two used mortars differ, they are both relatively long lasting and are described in more detail for a better understanding of the experimental results. Mortar M1 gains its strength solely because of carbonation, while for mortar M3a, two processes are responsible for gaining strength: pozzolanic reaction and hydration. Slag, the use of which is growing increasingly in the restoration of architectural heritage, is a latent hydraulic binder (it possesses hydraulic properties when properly activated) and is not the classic pozzolan, although it has similar properties to pozzolan [12]. Basically, slag is a waste material, obtained as a byproduct in the production of iron. When granulated blast furnace slag is mixed with water, its initial rate of hydration is much lower than when the water is mixed with Portland cement. With the addition of alkali, Portland cement, or lime, the reaction accelerates (slag is activated). The products of the setting of the lime and lime slag mixture are calcium silicate hydrates (CSH phase) [13]. Although lime–pozzolana mortar's pozzolanic reaction takes place first and carbonation represents a complementary reaction, the subsequent rate and sequence of pozzolanic reaction and carbonation depends on the composition of the binder, pozzolanic reactivity, and curing conditions. Curing in moist conditions enables faster progression of the pozzolanic reaction, while curing under dry conditions improves the rate of carbonation. The degree of pozzolanic reaction is also affected by the carbonation, which consumes part of the lime and can thus influence the mechanical properties and the porosity of lime–pozzolana mortars [14]. Lime–cement mortars setting is a combination of hydration of cement and carbonation of lime. Hydration of cement always takes place before carbonation of lime and the degree of both depends on the curing conditions. The rate of cement hydration is increased by curing in moist conditions, while combined wet/dry curing conditions increases the level of lime carbonation. In comparison with reference cement mortars, lime–cement mortars exhibit higher porosity, lower compressive strength, and more ductile behavior [15]. Carbonation takes place even in two-year-old specimens [16]. The hardening process of lime–pozzolana mortars is also long [17,18]. Conditions in a climatic chamber have a favorable effect on both processes (wetting of specimens, air circulation, relative humidity between 40% and 60%). Since the overall porosity is reduced by the carbonation, measurements of the ultrasonic transition time can be used to evaluate its progression [19]. Measurements of the ultrasonic velocities (UVs) on mortar prisms M1 have shown that on 347-day-old specimens, the UVs were 8% higher compared to 181-day-old specimens, which shows that carbonation was still ongoing. For mortar prisms M3a, the UVs measured in the longitudinal direction on 346-day-old specimens compared to 185-day-old specimens remained approximately the same, but there was a reduction of 24% in the transverse direction. Such a reduction could be the consequence of increased porosity or damage in the structure of

mortar M3a [9]. The decrease of UV in the case of mortar M3a was due to a reduction of the porosity or change in the structure, which may result from the interaction between the carbonation and pozzolanic reaction or hydration, which were still ongoing and influence each other. An increase of UVs of 8% between 181- and 347-day-old specimens M1 can be used as an approximate evaluation of increasing the compressive strength between 180- and 360-day-old specimens, which is ranked in the frame of a 10% increment of older versus younger specimens. For future research and evaluation of the results, it would be more correct to test samples of the same age. In this way, the effect of a possible increment of the compressive strength (although potentially small) at ages of more than 180 days would be eliminated. For the construction of wallets, solid clay bricks of standard format (available on the Slovenian market) were chosen based preliminary research. F/T was carried out [20]. The typical cycle included the following phases:

- Cooling phase in the interval of 20–30 min with a decreasing temperature of +20 ± 3 °C to −15 ± 3 °C;
- Freezing phase in the interval of 90–100 min with a temperature of −15 ± 3 °C (duration of the first two phases must be 120 min);
- Thawing phase lasting 15–20 min with an increasing temperature of −15 ± 3 °C to +20 ± 3 °C;
- Spraying phase lasting 2 min with a water temperature of 18–25 °C;
- Draining phase lasting 2 min.

The results of the compressive tests of wallets M1 and M3a cured in normal conditions as well as those exposed to 50 and 150 F/T cycles presented in Tables 1 and 2 represent key data for modeling (average = mean and median value, standard deviation, and coefficient of variation for each variable). At each stage, 3 specimens were tested. Here, f^I_w and u^I_w represent the compressive stress and vertical displacement at the first crack, respectively; u_{wmax} is the vertical displacement at the achieved compressive strength f_{wmax}; E_w is the Young's modulus; and G_w shear modulus.

Table 1. Results of the compressive tests of the wallets M1 [9].

	f^I_w (MPa)	u^I_w (mm)	f_{wmax} (MPa)	u_{wmax} (mm)	E_w (MPa)	G_w (MPa)
			M1-normal conditions			
Average	2.06	0.25	6.18	1.22	1428	554
Median	1.95	0.24	6.01	1.23	1395	560
Stdev	0.34	0.04	0.49	0.24	150	155
CoV	16%	15%	8%	20%	10%	28%
			M1-50 F/T cycles			
Average	3.10	0.35	6.73	1.09	1730	632
Median	2.80	0.35	7.09	1.16	1799	640
Stdev	0.55	0.07	0.78	0.14	123	69
CoV	18%	19%	12%	13%	7%	11%
			M1-150 F/T cycles			
Average	5.32	0.73	7.55	1.18	1608	700
Median	5.37	0.72	7.07	1.20	1533	674
Stdev	0.90	0.06	1.52	0.09	131	68
CoV	17%	8%	20%	7%	8%	10%

2.2. Analytical Part

Fragility curves, which enable probabilistic risk assessments in the case of ductility deterioration and increased damage of brick masonry due to freeze-thawing cycles, are a novelty in this research. They are presented for the first time on the basis of a very complex mathematical model based on the combination of two research areas (artificial intelligence methods and probability analysis). The presentation of the whole demanding process of determining the fragility curves is not of primary importance in this article and cannot be

presented in a short and at the same time simple (easy to understand) form. Therefore, the interested reader should find additional and supplementary information in the cited literature.

Table 2. Results of the compressive tests of the wallets M3a [9].

	f^I_w (MPa)	u^I_w (mm)	f_{wmax} (MPa)	u_{wmax} (mm)	E_w (MPa)	G_w (MPa)
			M3a-normal conditions			
Average	4.12	0.18	11.89	0.75	3723	1432
Median	3.91	0.18	12.62	0.73	3677	1335
Stdev	0.68	0.02	1.56	0.06	534	261
CoV	16%	11%	13%	8%	14%	18%
			M3a-50 F/T cycles			
Average	3.74	0.16	11.08	0.92	3852	1380
Median	3.91	0.15	10.98	0.84	3745	1471
Stdev	0.43	0.02	0.67	0.18	323	466
CoV	12%	9%	6%	20%	8%	34%
			M3a-150 F/T cycles			
Average	4.86	0.31	10.74	0.96	2817	1115
Median	4.80	0.28	10.34	0.82	2795	1151
Stdev	1.47	0.11	0.49	0.22	112	211
CoV	30%	34%	5%	22%	4%	19%

Therefore, in this section, we briefly present a general mathematical framework of the proposed models in the form of formal (general) equations, which requires (partial) inference to artificial intelligence methods (neural networks, fuzzy logic) and probabilistic analysis, including sampling procedures. Note that the proposed framework is presented in such a way that it can be applied to regression analyses (which determine the general trends of the observed phenomena) and fragility curves (which enable probabilistic risk assessments of the observed phenomenon). Due to the complexity of the whole approach, only a very brief description is given here.

A statistical/probabilistic model, which is typically derived from the observed data and is presented in this paper, is a special class of mathematical models. Since it is non-deterministic, some or all of its variables do not have specific values but instead have probability distributions (i.e., some or all of the variables are of random nature). It should be noted that basically all of the phenomena in structural engineering have a random nature, but due to the complexity, they are often treated as deterministic systems. The behavior of masonry wallets during the F/T cycles (in the presented research, this is expressed in terms of the modulus of elasticity, ductility, and damage) can be determined by observing/measuring N wallets during the experimental testing. The mathematical description of the observation of one wallet during the testing, which simulates the F/T phenomenon, is called a model vector. As a result, the whole phenomenon can be described by a finite set of model vectors [21]:

$$\{\mathbf{X}_1, \ldots, \quad \mathbf{X}_n, \ldots, \mathbf{X}_N\} \tag{1}$$

It is assumed that the observation of one particular wallet can be described by a number of variables, which are treated as components of a model vector:

$$\mathbf{X}_n = \{q_{n1}, \ldots, q_{nl}, \ldots, q_{nD}; r_{n1}, \ldots, r_{nk}, \ldots, r_{nM}\}. \tag{2}$$

The vector $\mathbf{X}_n$ can be further composed of two truncated vectors $\mathbf{Q}_n$ and $\mathbf{R}_n$:

$$\mathbf{Q}_n = \{q_{n1}, \ldots, q_{nl}, \ldots, q_{nD}\} \mathbf{R}_n = \{r_{n1}, \ldots, r_{nk}, \ldots, r_{nM}\} \tag{3a}$$

where $\mathbf{Q}_n$ is complementary to vector $\mathbf{R}_n$ and therefore their concatenation yields the complete data model, vector $\mathbf{X}_n$. The prediction vector, too, is composed of two truncated vectors, i.e., the given truncated vector and the unknown complementary vector:

$$\mathbf{Q} = \{q_1, \ldots, q_l, \ldots, q_D\}\hat{\mathbf{R}} = \{\hat{r}_1, \ldots, \hat{r}_k, \ldots, \hat{r}_M\} \tag{3b}$$

The problem now is how an unknown complementary vector $\hat{\mathbf{R}}$ can be estimated from a given truncated vector $\mathbf{Q}$ and the model vectors $\{\mathbf{X}_1, \ldots, \mathbf{X}_n, \ldots, \mathbf{X}_N\}$, i.e., how, e.g., the ductility of wallet, μ, can be estimated from known input parameters (type of mortar, number of F/T cycles, Young's modulus etc.) and the available data collected in the database. In the case of a large amount of data (big databases), different methods can be applied. One of them is demonstrated in [22]. However, in the case of a small database, which is available for the F/T phenomenon discussed in this paper, a different approach should be applied. In order to obtain the typical trends with F/T cycles, for optimal estimation of $\hat{\mathbf{R}}$ in terms of one or two mechanical properties, the standard statistical polynomial fit is used in this (first) step. Two output parameters (M = 2), Young's modulus, E, and ductility, μ, are separately estimated as a function of two input parameters, F/T cycles (D = 2) any type of mortar *type M*. In this particular case, Equation (3a,b) can be written as:

$$\mathbf{Q}_n = \{n_n, typeM_n\}\mathbf{R}_n = \{E_n, \mu_n\} \tag{4a}$$

$$\mathbf{Q} = \{n, typeM\}\hat{\mathbf{R}} = \{\hat{E}, \hat{\mu}\} \tag{4b}$$

In the presented research, the estimates (i.e., functional relationship) of the variables $\hat{E}$ and $\hat{\mu}$ are determined by using standard nonlinear regression (see Section 3).

However, to obtain as much information as possible from the observed phenomenon, a combination of Latin hypercube sampling (LHS) and fuzzy logic approach is used next. While Latin hypercube sampling [23,24] is applied to obtain a reliable estimate of the statistical parameters for the probabilistic model, the fuzzy logic approach [25] is used to exploit the expert knowledge about the observed phenomenon (i.e., the influence of two mortars on the investigated mechanical properties). The latter approach can deal with the concept of partial truth, which enables the incorporation of soft logic and/or engineering knowledge into the mathematical models. In summary, $\hat{\mathbf{R}}$, in terms of fragility curves for the ductility and damage index, is estimated in this (second) step based on LHS data generated from the assumed probability density functions and their statistical parameters (mean, standard deviation, and coefficient of variation) of known input parameters of the phenomenon, including fuzzy logic. Note that in this case, the formal description of Equation (4a,b) remains the same, and only the finite set of model vectors (N_{fc}) increases significantly in this case due to the LHS ($N \ll N_{fc}$).

Optimal estimation of $\hat{\mathbf{R}}$ is carried out by applying the conditional average estimation (CAE) method [22]. Note that the proposed approach (which includes the application of LHS and fuzzy logic) takes into account the randomness and different uncertainties of the observed phenomenon of freezing and thawing. The fragility curve represents the probability curves of the F/T phenomenon. More specifically, the fragility curve of the F/T phenomenon is defined as the conditional probability of exceedance for given values of the selected demand parameter (i.e., μ) using the general definition [26,27]. The fragility curves can, therefore, be obtained by a series of reliability analyses (i.e., calculation of the cumulative probability density functions for the mechanical property under consideration, taking into account all uncertainties) at varying demand thresholds. By ignoring the uncertainty in the demand [26,28], each fragility curve displays the probability that the actual mechanical property is less than or equal to a particular demand for this property.

3. Results

3.1. General Model

3.1.1. Regression Curves

In a useful and effective mathematical model that describes the real phenomenon, it is necessary to deal with two broad types of uncertainties [28]: aleatory uncertainties (also called inherent variability or randomness) and epistemic uncertainties. The former (aleatory) uncertainties are those that are inherent in nature or processes and cannot be influenced neither by the observer nor the manner of the observation. Such kind of uncertainty is present in the input variables of the F/T phenomenon as randomness in the F/T cycles, used material, quality of production etc. In contrast, the latter (epistemic) uncertainties are those that arise from our lack of knowledge. They stem from human choice to simplify matters, from errors in measuring observations, and last, but not least, from the finite size of the observation samples. They are typically present in the model parameters (i.e., chosen descriptive functions or relations between the variables). It should be noted that, whereas aleatory uncertainties are irreducible, epistemic uncertainties are reducible, e.g., by using improved models, more accurate measurements, and the collection of additional samples. However, in reality, it is hard to distinguish between both types; therefore, some simplifications are used when dealing with both types of uncertainties. Based on the experimental data, obtained by [9] and briefly described in Section 2.1, the following input parameters (independent variables) are used in the model under consideration, proposed in Section 2.2:

- Number of F/T cycles, described by a uniform variable;
- Type of mortar, described by a discrete variable, with 0 for lime mortar and 1 for lime mortar with blastfurnace slag additive.

As output parameters (dependent variables), Young's modulus and ductility are used.

Figure 1 shows the variation of Young's modulus, E_w, of wallets built of mortar M1 and M3a as a function of the number of F/T cycles. E_w of wallets M3a is, in principle, in the initial state before F/T, which is much higher compared to wallets M1. Before F/T, the average value of Young's modulus amounts to 3.72 MPa for wallets M3a and 1.43 MPa for wallets M1. Such results can be attributed to the stronger bond achieved between bricks and mortar in the case of mortar M3a regardless of the fact that mortar M3a was found to be weaker by the compressive and bending tests of mortar prisms. The importance and influence of the contact area between the brick and mortar on the compressive strength of the brick masonry walls has also been emphasized by other authors [29,30]. After 50 F/T cycles, Young's modulus for both types of wallets slightly increased, namely by 3.85 MPa for wallets M3a and 1.73 MPa for wallets M1. This is most likely due to favorable conditions for the setting in the climatic chamber. After 100 F/T cycles, the differences in terms of the trend of the change of the Young's modulus between the two types of mortar was clearly observed. For wallets M3a, the values were reduced at 3.55 MPa, while for wallets M1, there was a moderate increase at 1.79 MPa. Damage due to F/T apparently had no negative effect on wallets M1. In contrast, there was an increase in Young's modulus. On the other hand, for wallets M3a, the effect of damage after 100 F/T cycles was reflected in a reduction of Young's modulus. After 150 F/T cycles, there was a reduction of Young's modulus both by wallets M1 as well as wallets M3a, namely at 1.61 MPa for wallets M1 and 2.82 MPa for wallets M3a. The reduction rates as well as the trend shown in Figure 1 are typically higher for wallets M3a than wallets M1. The projection after 200 F/T cycles, which is based on the extrapolation based on graphs from Figure 1, shows about a 17% reduction for wallets M1 and a 56% reduction for wallets M3a compared to the initial values. Note that a low R-squared value (R^2) for wallets M1 generally indicates that the number of F/T cycles does not explain much of the variation of Young's modulus and thus may indicate low predictive acceptance of the proposed model. However, it is well known that even with low R^2 values, data with high variability can show a (significant) trend. As described above, the increase of Young's modulus at the beginning and the subsequent decrease has

a sound physical basis. On the other hand, the R^2 value for wallets M3a indicates moderate predictive acceptance for Young's modulus.

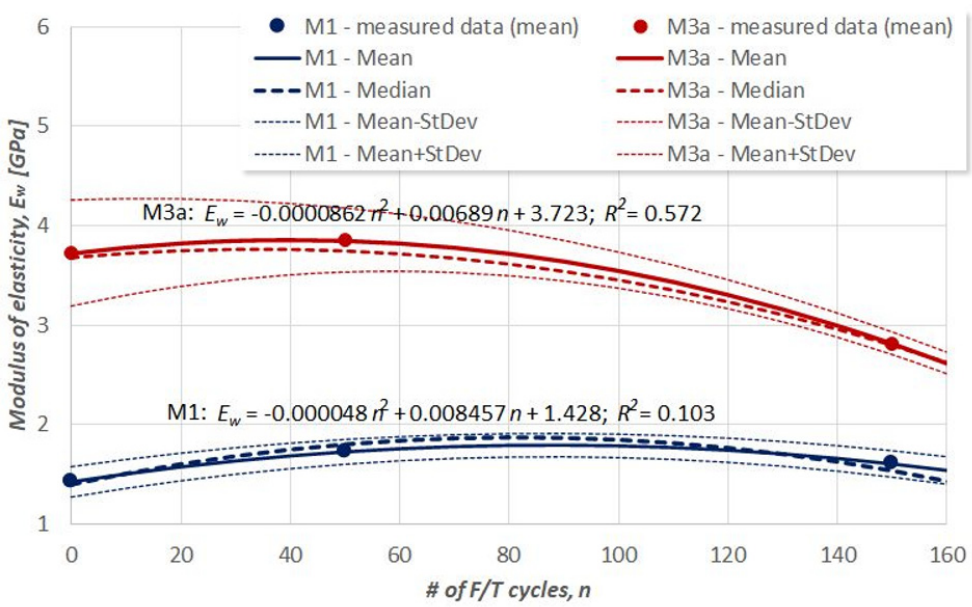


Figure 1. Mean and Mean ± Standard deviation regression curves for Young's modulus, E_w, for two types of mortar. Dashed line represents Median. Corresponding expressions for Mean are also presented.

Figure 2 shows variation of the ductility of wallets M1 and M3a as a function of the F/T cycles. Ductility is an important parameter, which can be correlated to damage [31], because contrary to Young's modulus, inelastic behavior is also considered. Ductility is usually defined as the ratio between the ultimate displacement (deformation) at which the force decreases to a certain level (90 or 80% of the maximum attained force) and the displacement at idealized limit of elasticity. However, analysis of the compressive strength tests of the individual wallets revealed (Tables 1 and 2) that in most cases, the compressive stresses did not decrease to 80% of the maximum attained level. The actual decreased compressive stresses were unrealistic due to local buckling and chipping of wallets and therefore, in those cases, ultimate displacements were estimated according to engineering judgement. Consequently, the ductility in the presented study was defined as the ratio between the maximum displacement, u_{wmax} (which is typically achieved at the estimated compressive stress higher than 80% of the maximum stress), and the displacement at the formation of the first crack, u^I_w. The ductility of the wallets that were not exposed to F/T cycles by both types of wallets was relatively comparable. After 50 F/T cycles, the ductility of wallets M1 decreased while the ductility of wallets M3a increased. After 150 F/T cycles both types of wallets showed relatively brittle behavior with the advancement of this trend, particularly for wallets M3a. The compressive strength of the wallets cured in normal conditions was determined on 202- to 207-day-old wallets, specimens exposed to 50 F/T cycles were tested at the age of 218 to 225 days, and specimens exposed to 150 F/T cycles at the age of 383 to 384 days. Note that a high R^2 value for wallets M1 and a low R^2 value for wallets M3a indicate high and low predictive acceptance for ductility, respectively. As with the Young's modulus, note that both derived relationships have a sound physical basis, and the quality of the predictive equations cannot be judged from the R^2 values alone.

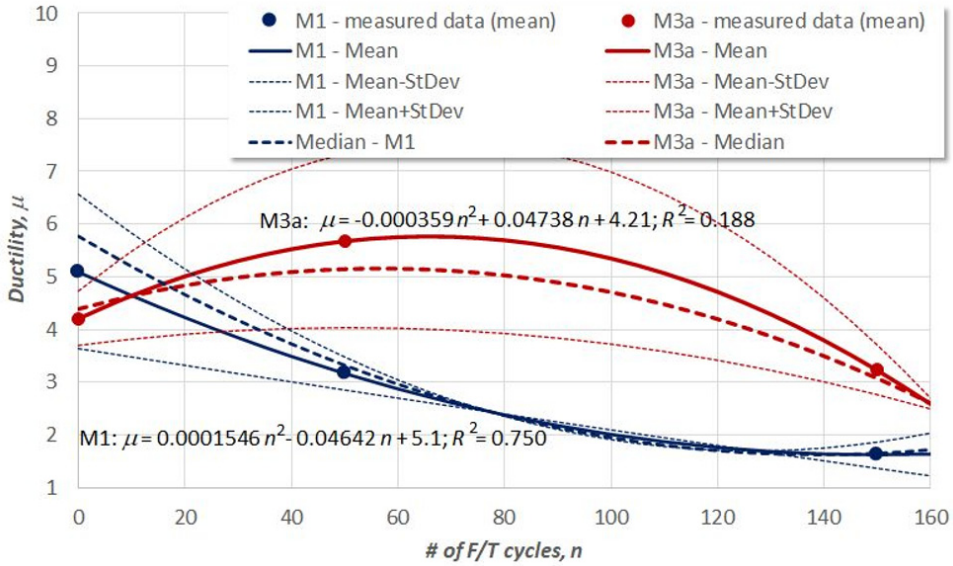


Figure 2. Mean and Mean ± Standard deviation regression curves for ductility, μ, for two types of mortar. Dashed line represents Median. Corresponding expressions for Mean are also presented.

3.1.2. Fragility Curves for Ductility

To construct fragility curves for the different mechanical properties in the presented study, we first chose the corresponding probability distributions and their coefficients of variations. Such data were needed for enlarging the database by using LHS.

For the F/T cycles, CoV was determined based on the different ages of the test specimens (see the description of the different sample ages) and the unreliability of a realistic description of the F/T cycles by the standard compared to the actual course in reality. This was a rough estimate, which is intentionally conservative, as separate experimental investigations would be needed for a more accurate estimate. The selected CoV value was 0.333 (i.e., 50 cycles/150 cycles). It contains equal proportions of epistemic (relatively (un)realistic protocol of F/T cycles compared to the real course in nature; different ages of samples in testing) and aleatory uncertainties (uncertainties in the implementation of protocols and measurements)!

For the mortar type, a relatively large value of 0.5 was deliberately chosen for the corresponding CoV. In this way, we consciously increased the influence of one mortar on another and consequently "smoothed" the influence of an individual mortar on the considered mechanical characteristics. Note that the fuzzy logic approach was simulated at this stage (the term simulation refers to the use of a Gaussian distribution instead of the triangular or trapezoid distribution commonly used and the standard fuzzy logic approach). At the expense of lower nonlinearity, we thus obtained more meaningful trends with the F/T cycles for the considered mechanical characteristics in both types of mortars. CoV contains mostly epistemic uncertainties due to simplifications of the influence of the mortar type.

Figure 3 shows the ductility fragility curves for walls M1 and M3a after 0, 50, and 150 F/T cycles, respectively. For comparison, the empirical (thin line), based on CAE analysis, and the corresponding theoretical fragility curves (bold line) obtained as cumulative distribution functions (cdf) are shown. For theoretical curves, the normal distribution was considered. An excellent match between the empirical and theoretical curves was observed, which is undoubtedly also due to the expansion of the database with the LHS method, where normal distributions were taken into account for all individual variables.

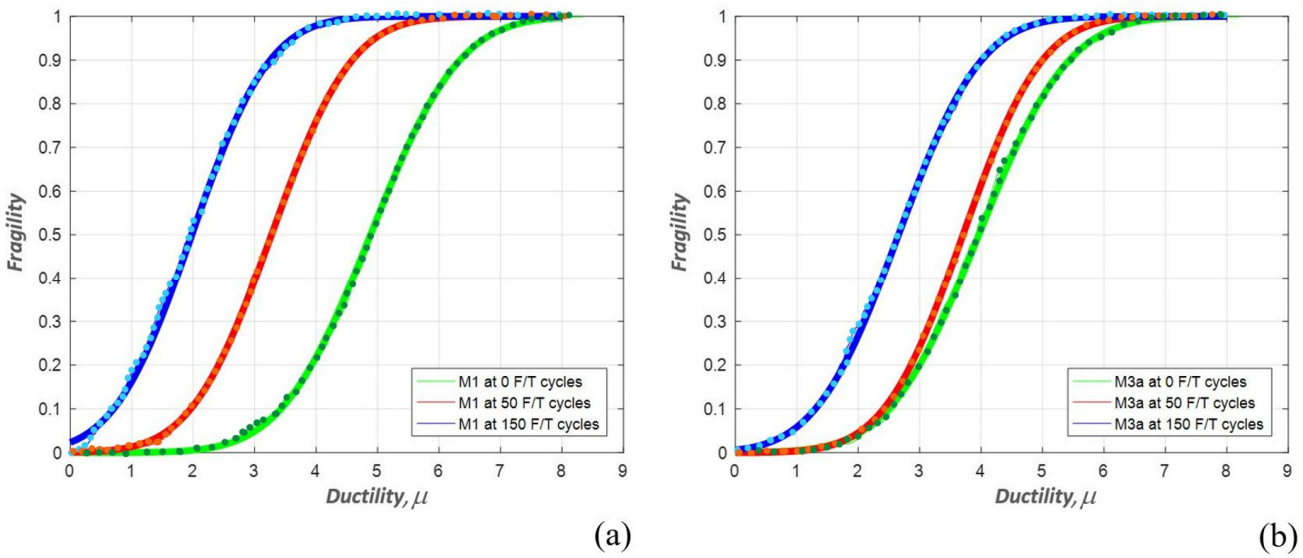


Figure 3. Fragility curves (assumption of normal probability distribution) for ductility for M1 (**a**) and M3a wallets (**b**). Note that bold lines correspond to theoretical cdfs, while dotted lines corresponds to the CAE estimation of cdfs.

3.2. Damage Model

3.2.1. Regression Curves

The damage model, proposed in this paper, is based on displacement ductility. Figure 4 demonstrates that the defined ductility can be effective in evaluating the masonry brick degradation under the F/T cycles. The probabilistic damage index of masonry brick wallets due to F/T cycles can therefore be expressed as [31,32]:

$$DI(n) = 1 - \frac{\mu(n)}{\mu_0}, \tag{5}$$

where $\mu(n)$ and μ_0 are the ductility of damaged (at n F/T cycles) and intact (unconditioned, at n = 0 F/T cycles) samples, respectively. Since, in some cases, μ_0 can be less than $\mu(n)$ (e.g., M3a at lower number of F/T cycles for standard approach), μ_0 is defined as μ_{MAX} and consequently the damage index is always less or equal than 1. Total damage is therefore represented by a value of 1.

For M3a wallets, two possible regression curves are shown. The variant with quadratic regression (dotted red line) corresponds to a monotonically increasing function, which can, however, very quickly exceed the maximal value of the damage index. Therefore, it makes sense to propose a variant with cubic regression (solid red line), which approximately asymptotically approaches the maximum value of the damage index.

3.2.2. Fragility Curves for Damage Index

The figures below (Figure 5) show the fragility curves of the damage index for wallets M1 and M3a after 0, 50, and 150 F/T cycles. Theoretical cdfs are shown for both the normal and log-normal probability distributions. The latter are shown for comparison, since highly non-linear phenomena, which is what the damage up to the failure is, typically correspond to a log-normal distribution. In both cases (normal and log-normal), the fragility curves for M3a wallets indicate much better resilience than M1 wallets (closer to the left).

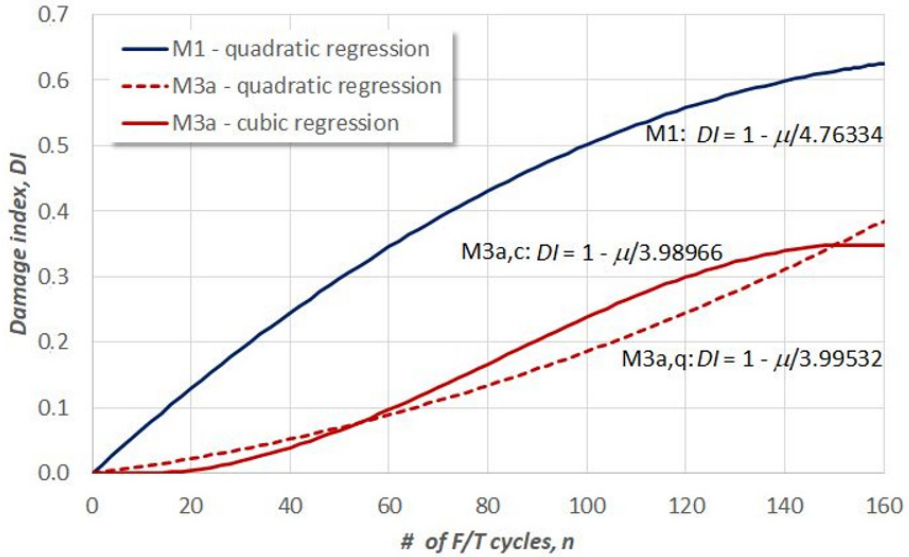


Figure 4. Damage index [DI] (Mean) as a function of the number of F/T cycles. Corresponding expressions for all three regressions are also presented. "c" and "q" denote cubic and quadratic regression, respectively.

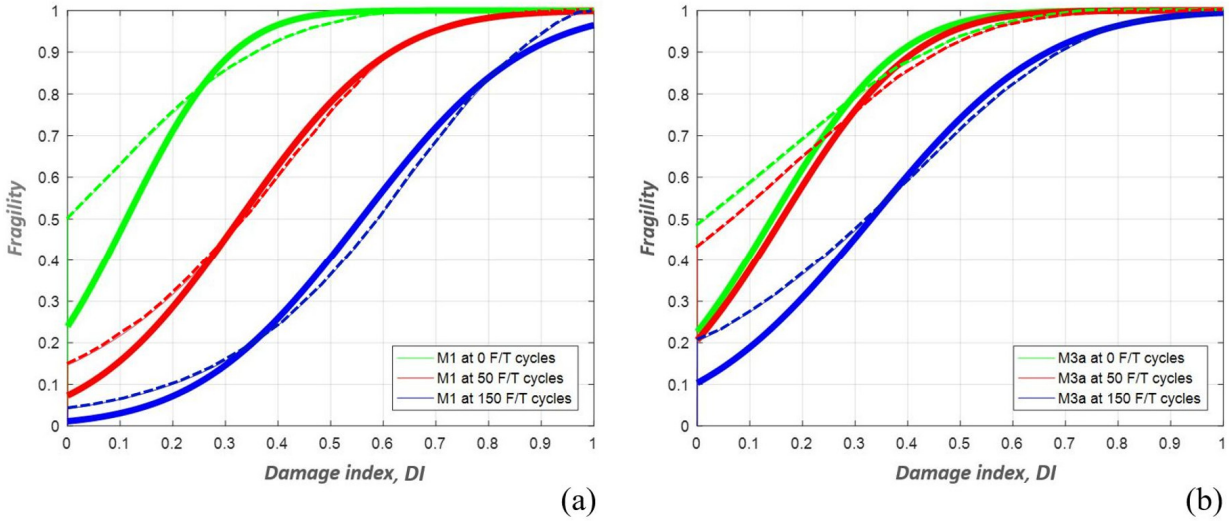


Figure 5. Normal and log-normal fragility curves for the damage index for M1 (**a**) and M3a (**b**) wallets. Bold and dashed lines correspond to the fitted theoretical cdfs based on the normal (bold) and log-normal (dashed) probability distributions, respectively.

4. Discussion

4.1. General Discussion

Brick wallets with two different mortars were experimentally tested for F/T cycles. The experimental results indicate (considerable) variability in the results between the observed wallets. We tried to determine the general trends with the number of F/T cycles for Young's modulus and for the ductility and fragility curves for the ductility and damage index.

The used analytical tools extend from the simple regression approach to the field of artificial intelligence, specifically to the field of neural networks. The relatively small database obtained from the experiments was expanded using the LHS method for more complex analyses. Since this is basically a probabilistic approach, which has recently become increasingly established in engineering assessments for the risk of building collapse and for risk assessments due to possible impacts on the environment, we took into account

the epistemic and aleatory uncertainties in the models. Consequently, the proposed models consider the CoV values obtained from the existing literature. The used CoV values are intentionally somewhat conservative (uncertainty is artificially increased in the modelling). In addition, CoVs include two basic types of uncertainty that are considered in a single value. Despite these simplifications, we believe that the results obtained are suitable for practical use.

In the case of the Young's modulus, we found similar trends in time for both types of mortar. It initially increased with time, despite F/T cycles, but later, its value began to decrease. The moderate increment of Young's modulus can be attributed to the favorable conditions for carbonation/hydration in the climatic chamber. Additionally, in first stage, the damage of the samples did not exhibit a significant effect on the results. It is important to point out that walls with improved mortar had, on average, a larger Young's modulus by more than a factor of 2. However, after reaching the maximum value, the decrease in the value of the Young's modulus was more pronounced than in the case of ordinary mortar.

In terms of ductility, the time trends for both types of mortar were significantly different than for the Young's modulus. The ductility of masonry with ordinary mortar was slightly higher in the initial state than the ductility of masonry with improved mortar. With an increasing number of F/T cycles, the ductility decreased monotonically and reached about one-third of the initial value at the final number of experimentally performed cycles. In contrast, in brick wallets with improved mortar, the ductility increased by about one-third at about 70 F/T cycles, but later began to decline and reached more than half of the initial value at the final number of experimentally performed cycles. In this case, we observed better ductility properties and behavior of the brick wallets with the improved mortar compared to the ordinary mortar. As the setting and thereby the increase in the compressive strength of both mortar types after 180 days was still ongoing, and as both hardening processes were positively influenced by the conditions in the climatic chamber, the results of the mechanical properties of the specimens cured in normal conditions and those after 50 and 150 F/T cycles were interpreted accordingly. A more realistic change of the mechanical parameters after 150 F/T cycles compared to 50 F/T cycles would have been obtained if the compressive strength tests were performed on the specimens of the same age. A downward trend of the evaluated mechanical parameters due to an increasing number of F/T cycles would thus be more obvious.

A favorable trend in the behavior of brick wallets with improved mortar was also observed in the case of the observed damage, expressed in terms of the damage index. The highest value of the damage index 1 means the worst damage. In the observed period (150 F/T cycles), the maximal achieved value of the damage index for a wallet with ordinary mortar was slightly more than 0.6, while for a wallet with improved mortar, this was about 0.35. Here, too, we observed a significantly more favorable behavior (greater durability) of the wallets with the improved mortar compared to the ordinary mortar. Therefore, we can assume that other types of mortars, such as lime-cement ones, which are most commonly used in Slovenia, or even hydraulic mortars, would give good or possibly even better results. With more resistant mortars, a longer lifespan of the walls would be achieved, indirectly resulting in a reduced amount of construction waste, which is in line with the principles of the circular economy. However, these assumptions should be confirmed by additional testing and analysis.

The obtained results of the fragility curves for ductility and for the damage index enabled probabilistic risk assessments in the case of unfavorable deterioration of ductility and/or an increase of damage due to F/T cycles. Fragility curves are somewhat conservative, but we still believe that they can enable realistic assessment of the risk of damage/collapse of masonry buildings for different scenarios of F/T.

The experimentally accelerated aging curves were constructed for two typical types of mortar. If such curves were also prepared for other types of mortar, they would undoubtedly be useful in determining the remaining life-span of a broad spectrum of masonry in

areas where such damage is likely to occur, thus making it easier to plan the necessary renewal and/or predict the remaining life-span.

4.2. Use Case

The experimental F/T tests performed in the laboratory were basically accelerated ageing tests that simulated the actual state in nature. Because these were simulations or approximations of the actual situation, the expected intervals of extreme temperature change that are predicted by standards were much shorter than intervals that occur in the real environment. The effect of F/T in the presence of water/moisture in the case when materials are saturated with water is much more problematic than the phenomenon of F/T alone. Such a situation can be critical for buildings, causing damage to mortar and bricks, which consequently affects the mechanical properties of the wall as a composite.

In the use case (Figure 6), we assumed that the life of the building was 100 years and that 150 F/T cycles were expected during that time. In fact, there may be more such cycles. The limitations of the basic study [9] on which the proposed mathematical models in this paper are based were implemented on water-saturated walls. In reality, this would mean that we are dealing with a completely saturated wall (e.g., due to flooding) that is subject to F/T.



Figure 6. Existing masonry brick building (mortar type M1) at the age of 70 years and corresponding localized damage after the assumed 105 F/T cycles analyzed for a hypothetical scenario.

Given the current age of the building (built with lime mortar type M1), which is 70 years, we assumed that it was exposed to at least 105 cycles of F/T in its lifetime. If we are interested in the expected state in 20 years, from the graphs in Figures 2 and 3, for the age of the building of 90 years (or 135 cycles), we can expect a 5.3% and 14.5% reduction in the Young's modulus and ductility (Figure 7).

For the observed building in the hypothetical scenario, we may also be interested in the probability that the damage will be limited (or acceptable) in the next 20 years (for the expected 135 F/T cycles). Since we are aware that the available data for the observed building are quite unreliable (note again that the demand is taken into account deterministically according to the basic definition of fragility curve), we require that the damage index should not exceed the value of 0.6. With a few iterations (we considered the linear interpolation between the proposed curves; see Figure 8), we arrived at the estimate that the probability for such an event is 0.62, which is a relatively high value (approximately in three cases out of five). If such a risk suits our needs, we can most likely plan appropriate renovation/remediation measures in 20 years. It should be noted, however, that in the

assessment, we assumed that there is a clear relation between the damage index and the actual damage, which ensures the effectiveness of the proposed fragility curves.

The proposed fragility curves provide different interpretations of the obtained results. In addition, by knowing the theoretical basis of the probabilistic approaches, they also offer us various quantitative answers related to risks connected to the management and maintenance of individual buildings or building stock (optimal planning of renovations and other measures).

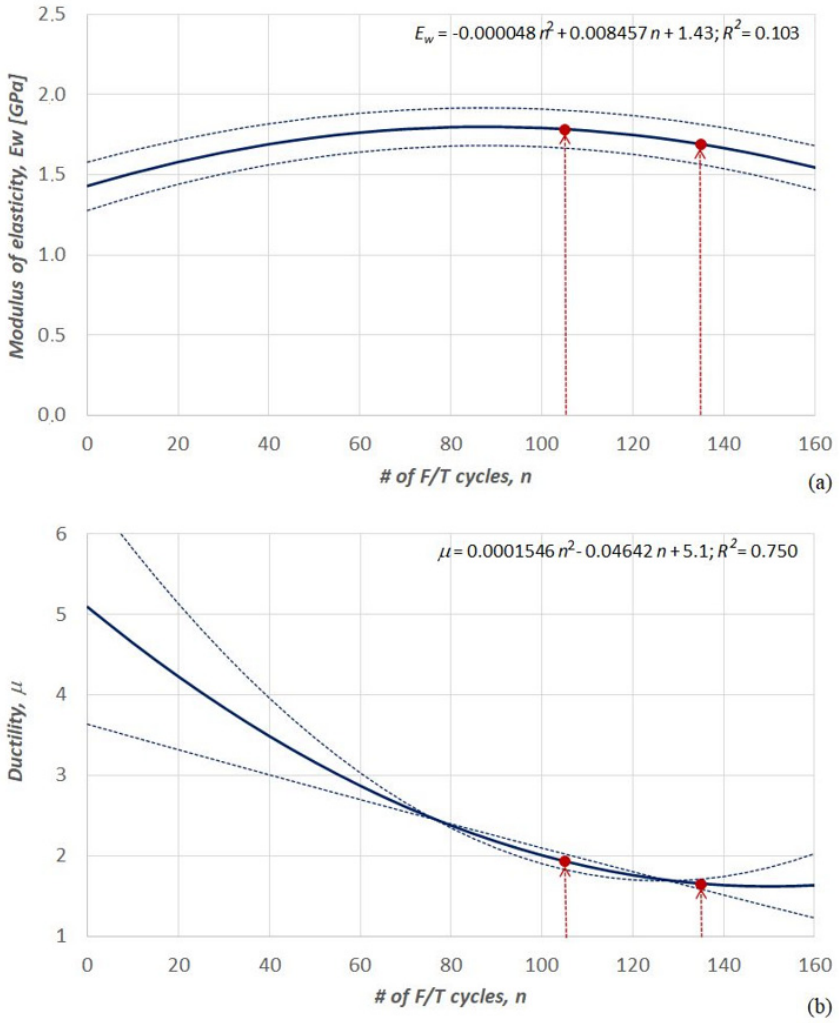


Figure 7. Predicted values for Young's modulus (**a**) and ductility (**b**) after 20 years for an existing masonry brick building in a hypothetical scenario. The graphs from Figures 2 and 3 were applied.

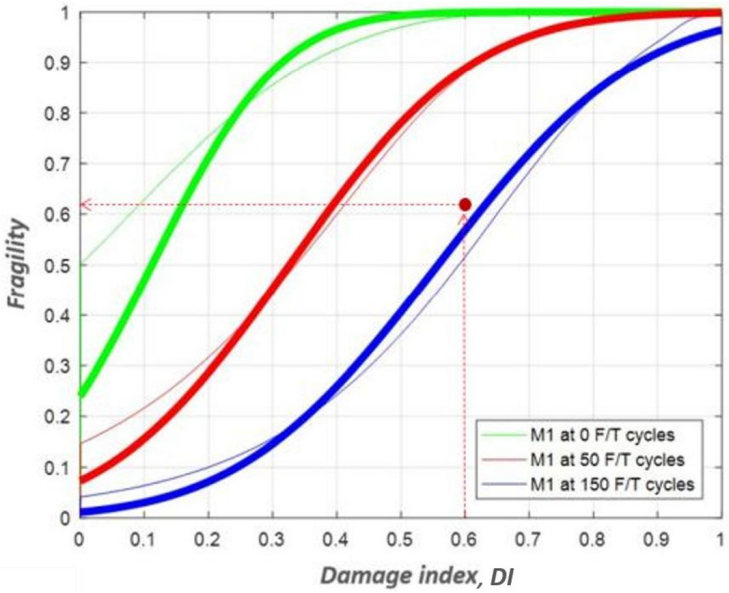


Figure 8. Estimated probability for the damage index, DI, not exceeding a value of 0.6 in 20 years for an existing masonry brick building in a hypothetical scenario. The graph from Figure 5 was applied.

5. Conclusions

The presented research investigated the F/T phenomenon of brick wallets that simulate structural elements (walls) of masonry buildings exposed to floods followed by cold weather. In an attempt to predict the progress of degradation and estimate the corresponding damage, mathematical models that can predict important mechanical parameters and damage for brick wallets for a given number of F/T cycles were developed. The proposed statistical regressions enable estimation of the deterioration of Young's modulus of elasticity and displacement ductility. Although the trends discovered have sound physical meanings, the low R^2 values for Young's modulus in the case of M1 wallets and for ductility in the case of M3a wallets suggest that the proposed regressions should be used with caution. In the first stage, the damage did not have a significant effect on Young's modulus. After 50 F/T cycles (M3a) and 80 F/T cycles (M1), the values began to decrease. Although wallets M3a built with improved mortar achieved significantly higher Young's modulus, its decrease was more pronounced compared to the wallets M1 built with the ordinary one. Regarding the ductility properties, somewhat better behavior was observed for the wallets built with the improved mortar. In addition, the proposed fragility curves for the ductility and damage index (which is an important novelty of the presented study) enabled probabilistic risk assessments in the case of deterioration of the ductility and increased damage of brick masonry due to F/T cycles. In terms of the damage index, wallets built with the improved mortar showed higher durability compared to ordinary ones, which is a good indicator of the development and usage of other types of modified mortars. A simple use case was also presented, demonstrating the usefulness of the proposed graphs. It was shown how the values of Young's modulus as well as the ductility at the selected age of a building exposed to F/T cycles can be obtained.

Author Contributions: Conceptualization, I.P. and M.U.; methodology, I.P.; software, I.P.; validation, M.U., I.P., M.S. and D.I.; formal analysis, I.P. and M.U.; writing—original draft preparation, I.P. and M.U.; writing—review and editing, M.U., I.P., M.S. and D.I.; visualization, I.P. and M.U.; supervision, M.U. and I.P.; project administration, M.U.; funding acquisition, M.U. All authors have read and agreed to the published version of the manuscript.

Funding: This research received no external funding.

Institutional Review Board Statement: Not applicable.

Informed Consent Statement: Not applicable.

Data Availability Statement: Source data that were further processed in this study can be found at https://repozitorij.uni-lj.si/IzpisGradiva.php?lang=slv&id=31805 (accessed on 1 August 2021).

Conflicts of Interest: The authors declare no conflict of interest.

References

1. Kokko, P.; Pentti, M. A New Freeze-thaw Method for Mortars Used in Nordic Climates. In Proceedings of the International RILEM Workshop on Repair Mortars for Historic Masonry, Delft, The Netherlands, 26–28 January 2005; pp. 187–195.
2. Powers, T.C. A working hypothesis for further studies of frost resistance. *J. Am. Concr. Inst.* **1945**, *16*, 245–272.
3. Fagerlund, G. Internal Frost Attack—State of the Art. In Proceedings of the RILEM Workshop Resistance of Concrete to Freezing and Thawing with or without De-Icing Chemicals, Essen, Germany, 22–23 September 1997; Setzer, M.J., Auberg, R., Eds.; RILEM: London, UK, 1997; pp. 321–338.
4. Powers, T.C.; Helmuth, R.A. Theory of volume changes in hardened Portland—Cement paste during freezing. In Proceedings of the Highway Research Board of the 32nd Annual Meeting, Washington, DC, USA, 13–16 January 1953; Volume 32, pp. 285–297.
5. Perrin, B.; Vu, N.A.; Multon, S.; Voland, T.; Ducroquetz, C. Mechanical behaviour of fired clay materials subjected to freeze–thaw cycles. *Constr. Build. Mater.* **2011**, *25*, 1056–1064. [CrossRef]
6. Stupart, A.W. A survey of literature relating to frost damage in bricks. *Masonry Int.* **1989**, *3*, 42–50.
7. Litvan, G.G. Freeze–Thaw Durability of Porous Building Materials. In *Durability of Building Materials and Components*; ASTM STP 691; Sereda, P.J., Litvan, G.G., Eds.; American Society for Testing and Materials: West Conshohocken, PA, USA, 1980; pp. 455–463.
8. Arizzi, A.; Viles, H.; Cultrone, G. Experimental testing of the durability of limebased mortars used for rendering historic buildings. *Constr. Build. Mater.* **2012**, *28*, 807–818. [CrossRef]
9. Uranjek, M.; Bokan-Bosiljkov, V. Influence of freeze-thaw cycles on mechanical properties of historical brick masonry. *Constr. Build. Mater.* **2015**, *84*, 416–428. [CrossRef]
10. Kralj, B.; Pande, G.N.; Middleton, J. On the mechanics of frost damage to brick masonry. *Comput. Struct.* **1991**, *41*, 53–66. [CrossRef]
11. Lindstrom, M. *Small Data—The Tiny Clues that Uncover Huge Trends*; St. Martin Press: New York, NY, USA, 2016.
12. Griffin, I. Pozzolanas as Additives for Grouts: An investigation of their working properties and performance charac-teristics. *Stud. Conserv.* **2004**, *49*, 23–34. [CrossRef]
13. Virgalitte, S.J.; Luther, M.D.; Rose, J.H.; Mather, B. *Ground Granulated Blast Furnace Slag as a Cementitious Constituent in Concrete*; ACI Report 233R-95; American Concrete Institute: Farmington Hills, MI, USA, 1995; p. 18.
14. Cizer, O.; Van Balen, K.; Van Gemert, D. Competition Between Hydration and Carbonation in Hydraulic Lime and Lime-Pozzolana Mortars. In *Advanced Materials Research*; Trans Tech Publications Ltd.: Bäch, Switzerland, 2010; Volume 133, pp. 241–246.
15. Cizer, O.; Van Balen, K.; Van Gemert, D. A Comparative Study of Hardening Reactions, Porosity and Mechanical Properties of Cement-Lime Mortars. In Proceedings of the 8th International Masonry Conference, Dresden, Germany, 4–7 July 2010; International Masonry Society: Shermanbury, UK, 2010; pp. 1133–1142.
16. Cazalla, O.; Rodriguez-Navarro, C.; Sebastian, E.; Cultrone, G.; de la Torre, M.J. Ageing of Lime Putty: Effects on Traditional Lime Mortar Carbonation. *J. Am. Ceram. Soc.* **2000**, *83*, 1070–1076. [CrossRef]
17. Hewlett, P.C. *Lea's Chemistry of Cement and Concrete, 4th ed*; Oxford Butterworth-Heinemann: Oxford, UK, 2004; p. 1057.
18. Moropoulou, A.; Bakolas, A.; Moundoulas, P.; Aggelakopoulpu, E.; Anagnostopoulou, S. Strength development and lime reaction in mortars for repairing historic masonries. *Cem. Concr. Compos.* **2005**, *27*, 289–294. [CrossRef]
19. Elert, K.; Rodriguez-Navarro, C.; Pardo, E.S.; Hansen, E.; Cazalla, O. Lime Mortars for the Conservation of Historic Buildings. *Stud. Conserv.* **2002**, *47*, 62–75.
20. SIST EN 772-1:2002. *Methods of Testing for Masonry Units—Part 1: Determination of Compressive Strength*; Institute for Standardization: Ljubljana, Slovenia, 2002; p. 11.
21. Grabec, I.; Sachse, W. *Synergetics of Measurement, Prediction and Control*; Springer Series in Synergetics; Springer: Berlin/Heidelberg, Germany, 1997.
22. Perus, I.; Poljansek, K.; Fajfar, P. Flexural deformation capacity of rectangular RC columns determined by the CAE method. *Earthq. Eng. Struct. Dyn.* **2006**, *12*, 1453–1470. [CrossRef]
23. McKay, M.D.; Beckman, R.J.; Conover, W.J. A Comparison of three methods for selecting values of input variables in the analysis of output from a computer code. *Technometrics* **1979**, *21*, 239–245.
24. Iman, R.L.; Helton, J.C.; Campbell, J.E. An approach to sensitivity analysis of computer models, Part 1. Introduction, input variable selection and preliminary variable assessment. *J. Qual. Technol.* **1981**, *13*, 174–183. [CrossRef]
25. Zadeh, L.A. Fuzzy sets. *Inf. Control* **1965**, *8*, 338–353. [CrossRef]
26. Zhu, L.; Elwood, K.J.; Haukaas, T. Classification and seismic safety evaluation of existing reinforced concrete columns. *J. Struct. Eng.* **2007**, *133*, 1316–1330. [CrossRef]
27. Perus, I.; Terčelj, M.; Kugler, G. Determination of scrap/supply probability curves for the mechanical properties of aluminium alloys in hot extrusion using a neural network-like approach. *Expert Syst. Appl.* **2012**, *39*, 5634–5640. [CrossRef]

28. Gardoni, P.; Der Kiureghian, M.A.; Mosalam, K.M. Probabilistic capacity models and fragility estimates for reinforced concrete columns based on experimental observations. *J. Eng. Mech.* **2002**, *128*, 1024–1038. [CrossRef]
29. Sarangapani, G.; Venkatarama Reddy, B.V.; Jagadish, K.S. Brick-Mortar Bond and Masonry Compressive Strength. *J. Mater. Civ. Eng.* **2005**, *17*, 229–237. [CrossRef]
30. Bosiljkov, V. Experimental and Numerical Research on the Influence of the Modified Mortars on the Mechanical Properties of the Brick Masonry. Ph.D. Thesis, Faculty of Civil and Geodetic Engineering, University of Ljubljana, Ljubljana, Slovenia, 2000; p. 314. (In Slovenian).
31. Chen, F.; Qiao, P. Probabilistic damage modeling and service-life prediction of concrete under freeze–thaw action. *Mater. Struct.* **2014**, *48*, 2697–2711. [CrossRef]
32. Lemaitre, J.; Desmorat, R. *Engineering Damage Mechanics: Ductile, Creep, Fatigue and Brittle Failures*; Springer: Berlin/Heidelberg, Germany, 2005.